WATER RESOURCES RESEARCH, VOL. 21, NO. 8, PAGES 1105–1115, AUGUST 1985

A Model for Steady Fluid Flow in Random Three-Dimensional Networks of Disc-Shaped Fractures

JANE C. S. LONG, PEGGY GILMOUR, AND PAUL A. WITHERSPOON

Earth Sciences Division, Lawrence Berkeley Laboratory, University of California, Berkeley

A model for steady fluid flow in three-dimensional, random networks of fractures has been developed. In this model the fractures are disc shaped discontinuities in an impermeable matrix. The fracture discs can be arbitrarily located within the rock volume and can have any desired distribution of aperture, radius orientation, and density. Thus where the disc model is appropriate it is possible to calculate flow through fracture networks which are statistically similar to those that occur in nature. After the boundary conditions and the desired fractures are specified, the intersections (nodes) between these discs (elements) are identified. Then steady flow through the network is calculated using a mixed analytical-numerical technique. In each fracture, analytic equations for flow into or out of each node as a function of the average head at each node are developed. The equations are based on image theory and the assumption that each node is a source (or sink) of uniform strength. A set of mass balance equations is constructed which equate flow into a node from one of its associated fractures to flow out of the node into the other associated fracture. These equations are solved for the average head at each node, and flux between fractures can then be calculated by substituting the average head values back into the analytical equations. The model has been successfully checked against analytical results for several cases of two and three intersecting fractures. We plan to use these techniques to measure the permeability of fracture networks.

INTRODUCTION

Analysis of fluid flow through large regions of fractured rock is usually performed by assuming that the fracture network behaves like a continuum on some scale. In this way, a block of rock on that scale can be characterized by a permeability tensor and the analysis of fluid flow can proceed in the same way that flow through porous media is analyzed. Previous work with two-dimensional fracture networks [*Long et al.*, 1982; *Long*, 1983; *Long and Witherspoon*, 1985; *Long et al.*, 1985] has demonstrated that such networks do not necessarily behave like continua. Techniques have been developed to determine (1) when a fracture network behaves like an equivalent continuum and (2) the components of a permeability tensor which minimize the error associated with performing an equivalent continuum analysis.

Such two-dimensional analysis has a limitation in that fractures which are not connected to the network in the plane of analysis may, in fact, be connected in the third dimension. Thus two-dimensional analysis will tend to underestimate the permeability and the network will appear to behave less like a continuum than it actually does in three dimensions. To overcome this limitation we have extended our techniques to three dimensions, and thus we developed a model to calculate steady fluid flow in random three-dimensional fracture networks.

CONCEPTUAL MODEL

The first step in developing a fracture flow model is to adopt a conceptual model for fracture networks which is compatible with the geometry observed in the field. Through the analysis of trace data and examination of fracture surfaces, several studies have reported that fractures are likely to be roughly elliptical or circular [*Baecher et al.*, 1978; *Robertson*, 1970; *Pollard*, 1976]. In this three-dimensional model we assume all fractures are circular. That is, we have adopted a subset of the general elliptical case mainly because the circular shape simplifies the calculation of flow. The extension of the mathematics to elliptical fractures is possible but not trivial. We further assume that the two opposite surfaces of the fractures are parallel and that a parallel plate model for flow is appropriate. Thus the model cannot account directly for channeling within the fracture planes. Head loss across the intersections between fractures and flow along the intersections are assumed to be negligible.

Although we are limited to circular fractures, the arrangement and size distribution of fractures in the model can be completely arbitrary. Several workers have contributed conceptual models for the arrangement of fractures in rock. *Conrad and Jacquin* [1973], *LaPointe and Hudson* [1981], *Veneziano* [1979], *Baecher and Lanney* [1978], and most recently *Dershowitz* [1984] have developed such conceptual models. For much of our work we use a model which is essentially the same as that developed by Baecher and Lanney in which circular fractures have lognormally distributed radii and are randomly located in space. Baecher and Lanney have supported this concept through analysis of trace data observed in outcrops, intersection data observed in boreholes, and the examination of fracture surfaces [*Baecher and Lanney*, 1978; *Robertson*, 1970; *Pollard*, 1976; *Hudson and Priest*, 1979]. A variety of fracture orientation distributions is possible and, in general, these distributions can be determined from field data [*Pincus*, 1953; *Mahtab and Yegulalp*, 1982; *Mahtab et al.*, 1972]. Arnold's hemispherical normal, Bringham's, Fisher's, and uniform distributions have all been used by various authors. Apertures can have lognormal distribution as was deduced by *Snow* [1969].

More complex statistical relationships between geometric parameters are also possible. *Long* [1983], *Long and Witherspoon* [1985], and *Long et al.* [1985] have pointed out that a correlation between aperture and fracture extent can account for the presence of "super conductors" which are commonly observed in the field. Others [*LaPointe and Hudson*, 1981; *Barton*, 1984] have observed that in some cases fractures occur in zones or bands of subparallel features. In other words, fractures may be spatially correlated. The presence of

Paper number 5W0341.
0043-1397/85/005W-0341$05.00

Fig. 1. Example of a three-dimensional fracture network of disc-shaped orthogonal fractures.

one fracture may increase the likelihood of there being another of the same set close by. Such fracture zones or super conductors may define the boundaries of blocks of rock which in turn may contain smaller features [*Conrad and Jacquin*, 1973; *Barton*, 1984]. Our flow model can accommodate any of the above features explicitly or stochastically. The only restriction at this time is that the fractures must be circular.

An example of such a random fracture system is shown in Figure 1. In this case three orthogonal sets of fractures have been drawn to simplify the illustration; in general, any orientation distribution is possible. Figure 2 shows a cubic region isolated from the system shown in Figure 1. A two-dimensional analysis of flow through this network would only include the traces of the fractures in a specified plane. Such a set of traces can be observed on any of the faces of the cube. Clearly, these traces do not interconnect to the same degree that the discs do. A two-dimensional analysis would greatly underestimate the permeability of this particular network. Much more realistic results can be obtained using this three-dimensional flow model.

SOLUTION OF THE FLOW EQUATION

We have not been able to find a general analytical solution for flow in large, random, three-dimensional fracture systems. On the other hand, in three dimensions, a purely numerical solution scheme such as used in the two-dimensional problem would require discretization within each fracture disc. While this is theoretically possible, this approach has two practical problems. The first is that the total number of unknowns would be equal to the number of fractures times the average number of elements in each fracture. Thus there would be severe limitations on the size of problem that could be analyzed. Secondly, the intersections between fractures are randomly located in the fracture disc. Thus the development of a numerical mesh generator to discretize every fracture would be difficult. The solution technique proposed here is a mixed numerical-analytical method. The flow relationships in each fracture plane are calculated analytically. The flux through the system is then calculated using a numerical solution based on the analytical solutions in each fracture and preserving mass balance in the system.

The analytical solution in each fracture plane is based on the assumption that each intersection acts like a source or sink with constant strength per unit line length (Figure 3). The fracture itself acts like a permeable disk with impermeable boundaries. Solution of the Laplace equation for this case consists of an equation for the potential distribution in the plane in terms of the total flux into or out of each of the intersections in any given fracture. The particular form of these expressions is determined by the particular geometry of intersections present in that fracture. From this equation we calculate the average head on each node in terms of the total fluxes. This results in a set of equations which can be inverted to produce an expression for the total flux into or out of each intersection in terms of the average head at each of the nodes.

These equations are developed in each fracture disc, and therefore two different expressions for the total flux into or out of each intersection will have been found for each node; i.e., one expression is found for each of the two fractures that form the intersection. A global mass balance equation can then be written by equating the flux into a node from one of its associated fractures to the flux out of the intersection into the other fracture. There will be one equation for each node. Solution of these equations gives the average head at each intersection. By knowing the average heads, the flux through each intersection can then be calculated using the solution to

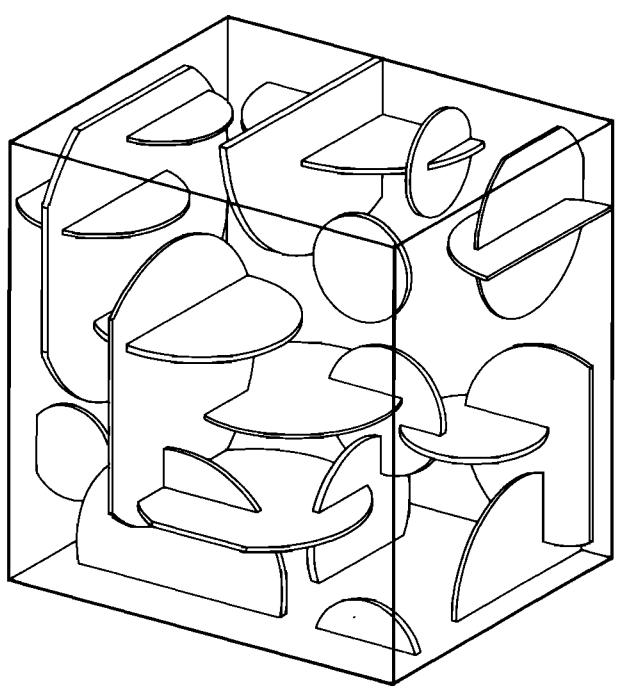

Fig. 2. Cubic region isolated from the network shown in Figure 1.

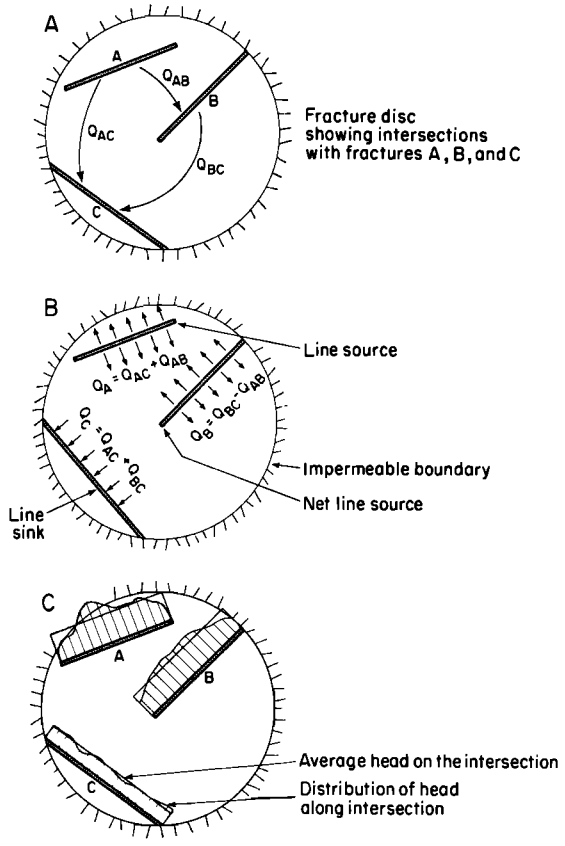

Fig. 3. Flow conditions in a fracture.

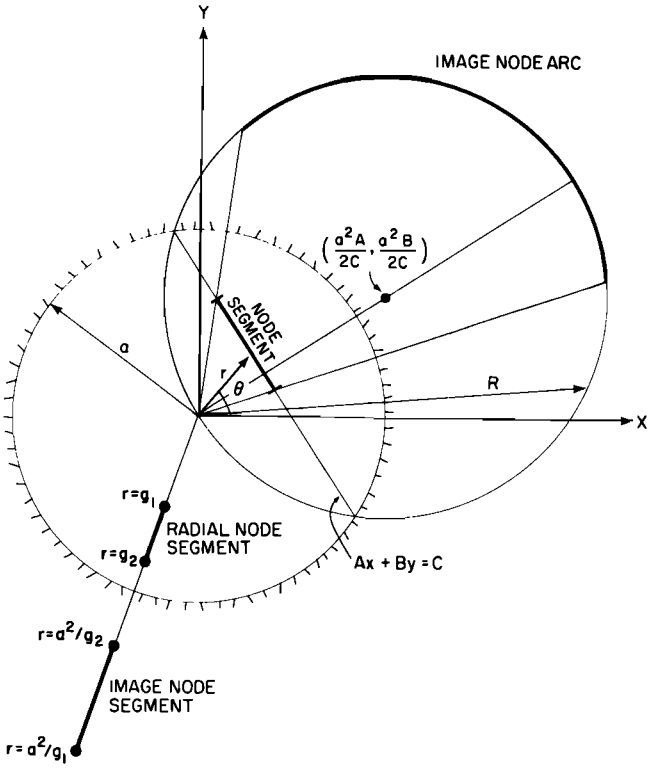

Fig. 5. Construction of the nodal images.

the Laplace equation which was developed for each fracture. The details of this process are given below.

The technique described here does not force the head distribution calculated on the intersection to be identical in both fractures, and we have assumed that the intersections are of constant strength per unit line length. In reality, the nodes will not have constant strength per unit line length, and the head distribution along the node must be the same as measured in either of the two intersecting fractures. We assume that the real total flux into or out of an intersection is approximately equal to the flux predicted with a source of constant strength per unit length. Furthermore, we require only the average head along the fracture intersection to be the same in each of the fractures which form the intersection. This means that solution accuracy should be improved by dividing each node into segments and treating each segment independently. In this way one can allow piecewise matching of average heads in the calculation of total flux at the expense of problem size. This concept is examined in the examples at the end of this paper.

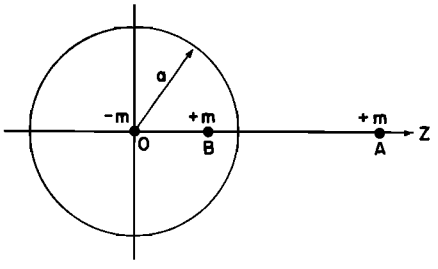

Fig. 4. Image system for a point source in a circle.

FLOW IN A FRACTURE DISC

Flow can only take place in a fracture if it is intersected by at least two other fractures. If a fracture is intersected by only one other fracture then it is a dead end which does not conduct fluid in steady flow. If a fracture is intersected by two other fractures, then within the fracture one of the intersections is (on the average) a line source and the other is (on the average) a line sink. We say "on the average" because flow within a given fracture may enter an intersection on one side and leave the intersection on the other. The net flow into or out of the intersection determines whether it is a source or sink for potential calculations. If the fracture is intersected by more than two other fractures, then at least one acts like a sink.

The solution of the problem of flow in a fracture disc uses image sources and sinks to account for the impermeable boundaries. In fact, the simplicity of the image system for a source or sink within a circle is a major advantage of assuming fractures are circular. The head distribution within a disc with impermeable boundaries containing an arbitrary number of line sources and sinks is based on the solution for a point source within a circular flow region. Consider a disc which contains a point source of strength $+m$ at B as shown in Figure 4. For steady state conditions *Milne-Thomson* [1968, p. 222] gives an image system which accounts for the impermeable boundary at $r = a$. If the source is located in the circle at B where $r = g$, then there is an image source of strength $+m$ on the same ray at A where $r = a^2/g$ and an image sink of strength $-m$ at $r = 0$. The head at any point in the fracture can be found by accumulating the head contributions of the source and the two images.

Recall at least two fracture intersections in a fracture disc are necessary to have steady flow in the disc, and at least one

of the intersections must act like a source and at least one must act like a sink. Furthermore, in order that the total flow into the fracture equals the total flow out of the fracture, the total strength of all sources must be equal and opposite to the total strength of all sinks. Therefore the total strength of all required images at $r = 0$ will always be zero.

Now we allow such point sources to be distributed along an arbitrary line segment (i.e., the node formed by the intersection of two fractures) in the circle such that the strength per unit line length is constant. First, we must find the locus of the distributed images. Then we must find the expression for the potential at any point in the fracture disc due to the sources along the intersection and along the image.

A nonradial line segment source will have an arc shaped image constructed as shown in Figure 5. A radial source will have a radial segment image. The equations for the locus of the arc and radial images can be derived as follows. The equation of the line on which the intersection lies can be given as $Ax + By = C$. Changing to radial coordinates, let $x = r \cos \theta$ and $y = r \sin \theta$. Then the equation is

$$Ar \cos \theta + Br \sin \theta = C$$

or

$$r = \frac{C}{A \cos \theta + B \sin \theta} \tag{1}$$

If $C \neq 0$, the equation of the image arc R is

$$R = a^2/r = (a^2/C)(A \cos \theta + B \sin \theta) \tag{2}$$

Returning to Cartesian coordinates, let

$$\cos \theta = x/R = \frac{x}{(x^2 + y^2)^{1/2}}$$

$$\sin \theta = \frac{y}{R} = \frac{y}{(x^2 + y^2)^{1/2}}$$

So we have

$$\left(x - \frac{a^2A}{2C}\right)^2 + \left(y - \frac{a^2B}{2C}\right)^2 = \frac{a^4}{4C^2}(A^2 + B^2) \tag{3}$$

Equation (3) is the equation of a circle centered at

$$\left(\frac{a^2A}{2C}, \frac{a^2B}{2C}\right) \qquad C \neq 0$$

with radius

$$\frac{a^2}{2}\frac{(A^2 + B^2)^{1/2}}{C}$$

and which always passes though the origin.

If the line segment is radial, $C = 0$, so

$$\theta = \tan^{-1}(-A/B) \tag{4}$$

is the equation of the image segment. The end points of the image segment are given by $r = a^2/g_1$ and $r = a^2/g_2$, where a is the radius of the fracture, and g_1 and g_2 are the distances from the end points of the intersection to the center of the fracture.

Now it remains to evaluate the potential distribution in the disc due to both the sources distributed on the intersection itself and the sources distributed on the image arc or radial segment. In the following $\phi_{iN}{}^k(X, Y)$ will be the potential due to the sources distributed along the intersection i in fracture k; $\phi_{iI}{}^k$ will be the potential due to the sources distributed along the image. Thus the potential due to the presence of intersection i is $\phi_i{}^k = \phi_{iN}{}^k + \phi_{iI}{}^k$. By superposition, the total potential due to all the intersections in the circle will be given by $\Phi^k = \Sigma_i\, \phi_i{}^k + C^kK^kb^k$, where C^k is the datum potential, K^k is the permeability, and b^k is the aperture of the fracture k. The average value of Φ^k on intersection i will be called $\bar{\Phi}_i{}^k$.

To be precise, this formulation for finding $\Phi_{iN}{}^k$ allows one to calculate the potential distribution due to the source node i at any point on the fracture except on the line source (or sink) itself where the potential is undefined. Thus $\bar{\Phi}_i{}^k$ is technically undefined, since $\phi_{iN}{}^k$ is not defined on i. This is a problem because for the global mass balance equations the only potentials we need are the average potentials at the intersections, i.e., $\bar{\Phi}_i{}^k$. We avoid this problem by assuming that the distribution of potential at any point not on the "line source" intersection can be calculated by assuming the intersections are line sources with no thickness. We then calculate the contribution of potential on node i due to node i by averaging the values of $\Phi_{iN}{}^k$ found a distance $\frac{w}{2}$ from the node, where w is the width of the node (w equals the aperture of the intersecting fracture divided by the cosine of the angle between them). By doing this we are essentially assuming the nodes are finite width sources (sinks) and we are forcing the potential distribution away from the source to match that of a source of infinitessimal thickness. Appendix A gives the calculation of average potential near the node due to the sources on the node and shows that in the limit as w approaches zero, $\bar{\Phi}_i{}^k$ remains finite.

Solution of the Laplace Equation in Each Fracture

The fundamental solution of the Laplace equation for the potential due to a point source in an infinite plane of transmissivity Kb is

$$\phi = Kbh = \frac{-Q}{2\pi} \ln r \tag{5}$$

where $m = Q$ is the strength of the source, r is the distance from the source, and h is the hydraulic head. We assume such sources are distributed over a line segment in the plane of length l. Now the potential in the plane due to the line source is given by

$$\phi_N = Kbh = \frac{-Q}{2\pi l}\int_0^l \ln r_p(\xi)\, d\xi \tag{6}$$

where $Q/l = m_\xi$ is the constant strength per unit line length, Q is the total strength of the line source, and r_p is the distance to any point in the plane. For each node we must specify $r_p(\xi)$ and evaluate the integral.

To find the potential contribution of the images, a similar integration is performed along the image of the node. In this case, however the strength per unit line length is not constant. For each infinitesimal piece of the intersection $d\xi$, the corresponding infinitesimal piece of image is ds. Now m_I, the strength per unit line length on the image, is given by

$$m_s = \frac{Q}{l}\frac{d\xi}{ds} \tag{7}$$

So potential due to the image is given by

$$\phi_I = Kbh = \frac{-Q}{2\pi l}\int_{S_1}^{S_2} \frac{d\xi}{ds} \ln r_p(s)\, ds \tag{8}$$

To evaluate this integral we must specify both $r_p(s)$ and $d\xi/ds$, or find $r_p(\xi)$ and change the limits of integration to $\xi(S_1)$ and

$\xi(S_2)$. The evaluation of (6) and (8) for the case of a nonradial node is given in Appendix B and for radial node in Appendix C. When the appropriate integrals have been evaluated, for each node in the fracture we have an expression for potential of the form

$$\begin{aligned}\phi_i^k &= \phi_{iN}^k + \phi_{iI}^k \\ &= Q_i f_{iN}^k(X, Y) + Q_i f_{iI}^k(X, Y) \\ &= Q_i F_i^k(X, Y)\end{aligned} \tag{9}$$

where $F_i^k = f_{iN}^k + f_{iI}^k$.

Image at the Center

The third potential term, ϕ_{io}, associated with intersection i is the potential due to an image of strength $-Q_i$ at the center of the fracture. However, as previously explained, the total strength of all such images at the center is zero, so no head is contributed from the sum of the images at the center.

Total Potential Field in the Fracture

The total potential in fracture k is given by

$$\phi^k(x, y) = \sum_{i=1}^{n} \phi_i^k + C^k K^k b^k = \sum_{i=1}^{n} (\phi_{iN}^k + \phi_{iI}^k) + C^k K^k b^k \tag{10}$$

where the i are the numbers of the intersections in fracture disk k. Equation (10) becomes

$$\Phi^k(x, y) = \sum_{i=1}^{n} Q_i F_i^k(X, Y) + C^k K^k b^k \tag{11}$$

The F_i^k represent shape functions for the total head distribution over the entire fracture due to the presence of the ith intersection. The average potential at each intersection, j, of fracture k due to the presence of intersection i is

$$\begin{aligned}\bar{\Phi}_j^k &= \frac{1}{l_j}\int_{l_j} \Phi^k(X, Y)\, dl_j + C^k K^k b^k \\ &= \frac{1}{l_j}\int_{l_j} \sum_{i=1}^{n} Q_i F_i^k(X, Y)\, dl_j + C^k K^k b^k \\ &= \sum_{i=1}^{n} \frac{Q_i}{l_j}\int_{l_j} F_i^k(X, Y)\, dl_j + C^k K^k b^k \\ &= \sum_{j=1}^{n} Q_i \mathcal{F}_{ij}^k + C^k K^k b^k\end{aligned} \tag{12}$$

where $\mathcal{F}_{ij}^k$ is the shape function for the average head on intersection j in fracture k due to the intersection i also on fracture k. That is,

$$\mathcal{F}_{ij}^k = \frac{1}{l_j}\int_{l_j} F_i^k\, dl_j \tag{13}$$

The value of $\mathcal{F}_{ij}^k$ may be difficult to obtain analytically, but it can be easily approximated by numerical integration. Recall that Appendix A shows how the average potential due to the contribution of the sources on node i can be calculated. That is, Appendix A shows how to evaluate

$$\frac{1}{l_i}\int_0^{l_i} \phi_{iN}\, dl_i$$

Solution of the Flow Equations

Equation (12) provides the potential distribution in each fracture as a function of the flux into or out of each node. In order to satisfy mass balance locally we note that the sum of the fluxes in a fracture element must be zero. Thus for n nodes on a fracture, there are $n-1$ independent values of Q_i. Using this fact, we invert (12) to obtain expressions for Q_i in terms of the $\bar{\Phi}_i$. When this is done for every fracture in the network, there are two independent expressions for each Q_i, since node i exists on both fractures forming intersection i. By equating each of these pairs we guarantee mass balance through the network. The set of equations equating flow into each intersection to flow out of each intersection can be solved for the $\bar{h}_i$. We solve for $\bar{h}_i$ rather than $\bar{\Phi}_j^k$ because the average potential, $\bar{\Phi}_j^k$, will have a different value in each of the two intersecting fractures if the transmissivity of the two fractures is different. The average total head at the node, $\bar{h}_j$, however, will be the same in both fractures. Values of Q_i can be found by substituting the $\bar{h}_i$ into either of the analytical solutions for Q_i developed for each of the fractures which intersect at i. The details of this technique are given below.

We first rewrite (12) in terms of head:

$$\bar{h}_j = \sum_{i=1}^{n} \frac{Qi}{K^k b^k} \mathcal{F}ij + C^k \tag{14}$$

For mass conservation in each fracture we have

$$\sum_{i=1}^{n} Q_i = 0 \tag{15}$$

By allowing

$$Q_N = -\sum_{i=1}^{n-1} Q_i \tag{16}$$

and substituting (16) into (14)

$$\bar{h}_j = \sum_{i=1}^{n-1} \frac{Q_i}{K^k b^k}(\mathcal{F}_{ij}^k - \mathcal{F}_{Nj}^k) + C^k \tag{17}$$

for $j = 1, n-1$. We eliminate the constant C^k by subtracting $\bar{h}_{j+1}$ from $\bar{h}_j$:

$$\begin{aligned}(\bar{h}_j - \bar{h}_{j+1}) = \sum_{i=1}^{n-1} \frac{Qi}{K^k b^k} [(\mathcal{F}_{ij}^k - \mathcal{F}_{nj}^k) \\ - (\mathcal{F}_{ij+1}^k - \mathcal{F}_{Nj+1}^k)]\end{aligned} \tag{18}$$

Letting

$$(\mathcal{F}_{ij}^k - \mathcal{F}_{Nj}^k) - (\mathcal{F}_{ij+1}^k - \mathcal{F}_{Nj+1}^k) = \zeta_{ij}^k \tag{19}$$

$$(\zeta^k)^{-1} = \mathcal{G}_{ij}^k \tag{20}$$

we have

$$Q_i = \sum_{j=1}^{n-1} \mathcal{G}_{ij}^k K^k b^k [\bar{h}_j - \bar{h}_{j+1}] \tag{21}$$

for $j = 1, n-1$, and from (16)

$$Q_N = -K^k b^k \sum_{i=1}^{n-1}\sum_{j=1}^{n-1} \mathcal{G}_{ij}^k (\bar{h}_j - \bar{h}_{j+1}) \tag{22}$$

We now use (21) and (22) to write the global mass balance equations as described below. The global mass balance equations can be solved for all the values of $\bar{h}_j$. When these are known, the values of Q_i can be found by substitution into (21) and (22). The value of C can be obtained by substituting $\bar{h}_j$ and Q_i into (14).

Global Mass Balance Equations

Two versions of (21) or (22) are written for each intersection, once for each fracture associated with the intersection. For

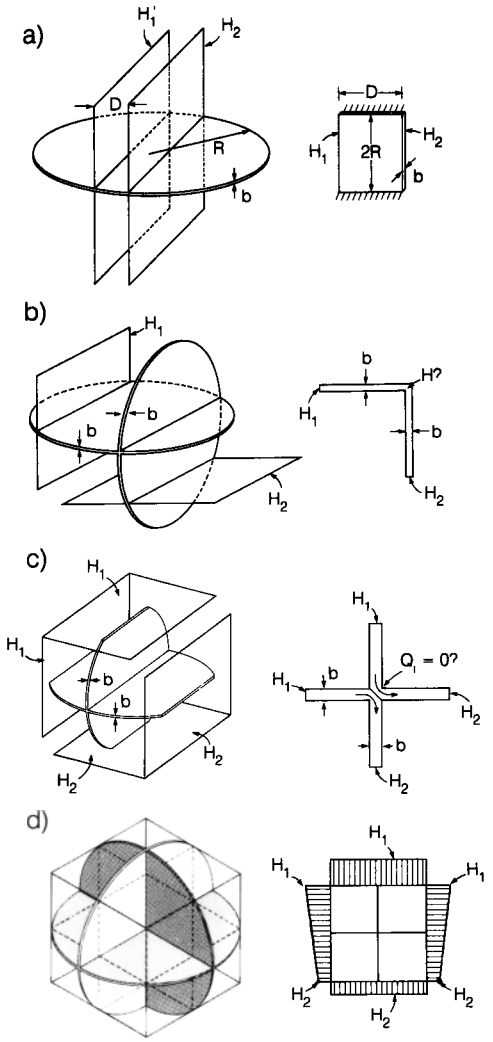

Fig. 6. Example of applications for (*a*) one fracture intersecting two parallel boundary planes; (*b*) two equidimensional intersecting fractures, each intersecting one boundary; (*c*) two equidimensional intersecting fractures, each intersecting two boundaries; (*d*) three equidimensional, orthogonal fractures of radius r which intersect symmetrically and are truncated by a boundary cube of dimensions $\sqrt{2}r \times \sqrt{2}r \times \sqrt{2}r$.

example, if fracture k and fracture p intersect at i, then the fact the flow enters k from p (or vice versa) through i can be expressed by

$$\sum_{j=1}^{J-1} \mathcal{G}_{ij}{}^{k} K^{k} b^{k} [\bar{h}_j - \bar{h}_{j+1}] + \sum_{m=1}^{M-1} \mathcal{G}_{im}{}^{p} K^{p} b^{p} [\bar{h}_m - \bar{h}_{m+1}] = 0 \tag{23}$$

where j and m have global numbers which correspond to local numbering $j = 1, J$ and $m = 1, M$, respectively, when there are J nodes on fracture k and M nodes on fracture p. If node i is the Mth node on p or the Jth node on k, then we use (22) instead of (21) to form (23). We write one equation (23) or its equivalent for each node in the network.

Boundary Conditions

If a fracture intersects a boundary, the intersection is called a boundary node. In this case we can assign a constant head to the node by substituting the following equation for (23):

$$\bar{h}_j = H_j \tag{24}$$

where H_j is the appropriate constant.

Constant flux boundaries can be accommodated by substituting (21) or (22) for (23), where Q_i in this case is the specified flux through the boundary node.

When all these equations have been assembled, expanding and collecting terms gives an equation of the form

$$A_{ij} \bar{h}_j = b_j \qquad i, j = 1, NN \tag{25}$$

where summation is implied by repeated indices, and NN is the number of nodes in the network. The vector b_j is nonzero only for nodes j which are boundary nodes. The matrix A_{ij} is symmetric and sparse, and the bandwidth can be minimized by appropriate node numbering. Inversion of A_{ij} allows calculation of $\bar{h}_j$, which in turn allows calculation of Q_i through (21) and (22) and calculation of C^k through (14).

Example Applications

The following section describes five examples that were among those used to verify the computations performed by the model described in this paper. The first four cases are illustrated in Figure 6. The left-hand side of each illustration shows the case solved by the three-dimensional flow program. On the right in each case is shown the corresponding analytical case used for comparison. The fifth case is a random case where no analytical solution is available, this case has been presented to compare the results using different discretization schemes on the intersections. No figure is available to illustrate this case. The results presented below are dimensionless for consistent units.

Case 1: One Fracture Intersecting Two Parallel Boundary Planes

This is the simplest case possible; if the boundaries are centered and closely spaced relative to the radius of the fracture, the flux in the fracture is approximately equal to the linear flow in a rectangular slab of thickness b between two constant head boundaries as shown in Figure 6*a*. In this case we are only checking the calculation of flux because both nodes are boundary nodes with assigned heads. The flux between the nodes in the numerical case is 4.968 for $H_1 = 1.0$, $H_2 = 0.0$, unit transmissivity, fracture radius equal to 5.0, and the distance between the constant head boundaries equal to 2.0. In the analytical case, for a slab of dimensions 2.0 × 10.0, where 10.0 matches the diameter of the fracture, the flow is 5.0. For a slab 9.798 × 2.0, where 9.798 matches the length of the nodes on the fracture, the flow is 4.899. Thus the analytical results bound the numerical results as expected.

Case 2: Two Equidimensional Intersecting Fractures, Each Intersecting One Boundary

In this case (Figure 6*b*) we expect the average head on the intersection between the two fractures to be the average of the heads on the two boundary nodes and by symmetry we expect the total flux into or out of each node to be equal in magnitude. For the case of $H_1 = 1.0$, $H_2 = 0.0$, fracture radius = 5.0, unit transmissivity, and a distance of 8.0 between the intersections, the numerical results were $Q = +0.4949$ for each inflow node and $Q = -0.4949$ for each outflow node, and the average head at the intersection between the fractures was 0.5000.

Case 3: Two Equidimensional Intersecting Fractures, Each Intersecting Two Boundaries

This case is designed to check the calculation for net flux at an intersection when, in the plane of the fracture, flow is en-

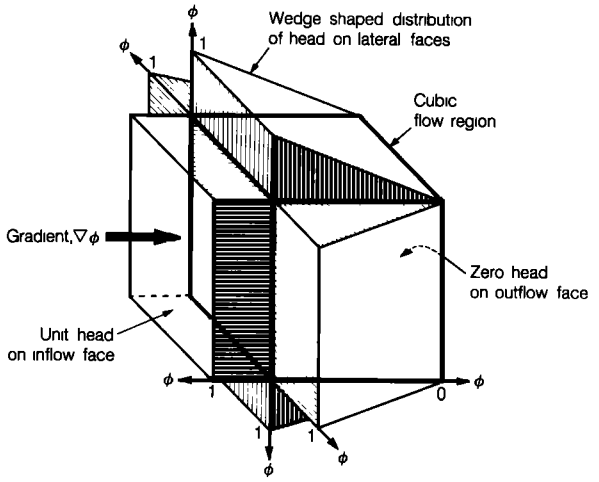

Fig. 7. Boundary conditions used to produce a constant gradient.

tering the intersection on one side and leaving the intersection on the other. For the symmetric case shown in Figure 6c, the head at the center intersection should be $(H_1 + H_2)/2$ and the total flux at the intersection between the two fractures should be zero because an equal amount of flux is entering this node on one side as is leaving it on the other. In fact, for $H_1 = 1.0$ and $H_2 = 0.0$ the numerical results give $Q = 0.0$ and $H = 0.5000$ at the center node.

Case 4: Three Equidimensional, Orthogonal Fractures of Radius r Which Intersect Symmetrically and are Truncated by a Boundary Cube of Dimensions $\sqrt{2}r \times \sqrt{2}r \times \sqrt{2}r$

In this case (Figure 6d), we apply the boundary conditions of the form illustrated in Figure 7. These boundary conditions induce a constant gradient in the two fractures which are perpendicular to the inflow face. There is zero gradient in the fracture parallel to the inflow face; thus this fracture experiences no flow. The boundary conditions inducing flow on the two fractures which are perpendicular to the inflow face are illustrated on the right-hand side of Figure 6d. An analytical solution provides us with the flux into each of the boundary nodes on these fractures. Also, from symmetry considerations, we should have $H = (H_1 + H_2)/2$ and $Q = 0.0$ on all of the internal nodes. In this case, we subdivided the nodes in various ways to determine the effect on accuracy. In all cases, the conditions on the internal nodes were satisfied, but the different schemes for dividing the nodes produced slightly different values for flux into the boundary nodes on the inflow surface (which must be equal to the flux out of the corresponding boundary nodes on the outflow surface).

For $r = 71.0$, $\sqrt{2}r = l = 100.0$, transmissivity $= 0.8172 \times 10^{-5}$, $H_1 = 1.0$ and $H_1 = 0.0$, the flux through the inflow or outflow face of the cube should be

$$Q_T = nKbl\left(\frac{H_1 - H_2}{l}\right)$$

$$= 2(0.8172 \times 10^{-5} \times 100 \times 1.0/100)$$

$$= 0.1634 \times 10^{-4}$$

where $n = 2$ because two fractures intersect the inflow (and outflow) face. The numerical results for Q_T, the total flux through the inflow face, are shown in Table 1. Two different discretization schemes were used. The first was to divide each node (boundary and internal) into a number of equal segments (2, 3, 4, or 10). The second is to divide only the boundary nodes into equal segments and leave the internal nodes intact.

As is shown in Table 1, dividing the nodes into segments improved the accuracy, and most of the improvement was achieved with the first division from one to two segments. The results obtained for dividing only the boundary nodes are exactly the same as the results obtained for dividing all the nodes. Hence dividing the internal nodes had no effect at all on accuracy. If this were true, in general, it would be good because we wish to minimize the number of unknowns. However, this particular case is symmetric and each internal node is truncated by boundary nodes at both ends. So, we look at a more general case below.

Case 5: 10 Randomly Located and Randomly Sized Fractures

In this case, 10 fractures were randomly generated and again truncated by the cubic boundaries shown in Figure 7. These fractures formed 38 nodes, including 18 internal nodes and 20 boundary nodes. This case was also used to study the effect of nodal discretization. However, being a random case, no analytical solution is available to check the results. We made the assumption that the "true flux" is closest to the flux calculated when all the nodes are divided into 10 equal segments. The results for less than 10 segments on some or all nodes are then compared to this case.

In this case there is flow entering or leaving all six faces of the boundary cube. In general, we again see an improvement in accuracy for head and flux with increasing discretization. The results obtained for discretizing only the boundary nodes are slightly different from the results obtained when all of the nodes are discretized. In order to minimize problem size and still maintain accuracy, it appears to be more efficient to subdivide the boundary nodes and not subdivide the internal nodes. Based on case 5, one might decide to discretize only the boundary nodes into three segments because this scheme seems to achieve the most accuracy for the smallest increase in problem size. However, further investigation is needed to confirm this as the best scheme under all circumstances.

CONCLUSION

An efficient model is available for calculating steady flow through networks of disc-shaped fractures which can be of any size and arrangement. It will be important to develop plotting schemes to draw these fractures in three dimensions, much as the illustration in Figure 1 was drawn by hand. In this way we can more easily understand the physical responses we observe in the network. We intend to use this model to study the permeability of three-dimensional fracture networks much as we have studied two dimensional systems [*Long et al.*, 1982; *Long*, 1983; *Long and Witherspoon*, 1985; *Long et al.*, 1985].

Extension of the image construction to elliptical fractures would involve a Joukowski transformation [*Milne-Tompson*, 1968]. This is theoretically possible, but complex. An extension three-dimensional model to permit analysis of transient flow is also envisioned.

TABLE 1. Total Flux Through the Fracture Network in Case 4 as a Function of Nodal Discretization Scheme

Number of Segments	Total Flux $\times 10^{-4}$*
1	0.1982
2	0.1705
3	0.1679
4	0.1665
10	0.1647

*All nodes segmented or only boundary nodes segmented.

APPENDIX A

Calculation of Average Potential Near a Finite Line Source

When we wish to calculate the average of total potential on a given intersection, we can easily evaluate the potential contribution due to all the other intersections and their images on the intersection of interest. However, the contribution of the intersection itself cannot strictly be obtained in the same way because the potential due to the source is not defined on the source itself. Hence we derive an expression for the average potential on a line segment parallel to the line source a short distance, $\pm\varepsilon$, away from it.

The potential contribution due to a point source is given as

$$\phi(x, y) = -\frac{Q}{2\pi} \ln r \tag{A1}$$

where r is the distance to the point (x, y). As in (6), we integrate a series of such sources, each of strength $Q/l\ d\xi$ along a line segment on the x axis, $0 \le x \le l$, to obtain the potential due to a line source:

$$\phi(x, y) = -\frac{Q}{2\pi l} \int_0^l \ln [y^2 + (x - \xi)^2]^{1/2}\ d\xi \tag{A2}$$

where r is now equal to $[y^2 + (x - \xi)^2]^{1/2}$. Integrating, we have

$$\phi(x, y) = -\frac{Q}{4\pi l}\left\{(l - x) \ln [y^2 + (x - l)^2] - 2l + 2|y| \tan^{-1}\left(\frac{l - x}{|y|}\right) + x \ln [y^2 + x^2] - 2|y| \tan^{-1}\left(-\frac{x}{|y|}\right)\right\} \tag{A3}$$

We now examine the average value of ϕ on a line segment at $y = \pm\varepsilon$ and $0 \le x \le l$:

$$\bar{\phi} = \frac{1}{l} \int_0^l \phi(x, \varepsilon)\ dx$$

$$\bar{\phi} = -\frac{Q}{4\pi l^2}\left[(l^2 - \varepsilon^2) \ln (l^2 + \varepsilon^2) - 3l^2 + 4l|\varepsilon| \tan^{-1} \frac{l}{|\varepsilon|} + \varepsilon^2 \ln \varepsilon^2\right] \tag{A4}$$

Equation (A4) can be used to evaluate the potential contribution of the source on itself by allowing ε to take the value of $\frac{w}{2}$, where w is the width of the intersection. However, if ε is very small we can use the expression

$$\bar{\phi} = -\frac{Q}{4\pi l^2}(l^2 \ln l^2 - 3l^2) \tag{A5}$$

because

$$\lim_{\varepsilon \to 0} (\varepsilon^2 \ln \varepsilon^2) = \lim_{\varepsilon \to 0} \frac{f(\varepsilon)}{g(\varepsilon)} = \lim_{\varepsilon \to 0} \frac{f'(\varepsilon)}{g'(\varepsilon)} = \lim_{\varepsilon \to 0} \frac{2 \ln \varepsilon}{\varepsilon^2} = \lim_{\varepsilon \to 0} \frac{2\varepsilon^{-1}}{-2\varepsilon^{-3}} = 0$$

by l'Hospital's rule.

APPENDIX B

Nonradial Intersections

Consider a nonradial intersection (Figure B1). A local arbitrary X, Y coordinate system is established for each fracture disc. All the equations for potential distribution must be referred to X, Y coordinates before they are added. Coordinates concenient for calculation are the x', y' coordinates shown on Figure B1. These coordinates are centered at one end point of the intersection. The y' axis lies on the intersection. Point 0 is the center of the fracture. Point P is an arbitrary point in the plane. Equation (6) becomes

$$\phi_{iN}{}^k = K^k b^k \bar{h}_{iN} = \frac{Q_i}{2\pi l_i} \int_0^{l_i} \frac{1}{2} \ln [x'^2 + (y' - \xi)^2]\ d\xi \tag{B1}$$

where $Q_i/l = m_\xi$ is the strength per unit line length, Q_i is the total strength of the line source, and $r_p = [x'^2 + (y' - \xi)^2]^{1/2}$. The subscript i refers to intersection i. This integral has been evaluated in the work by *Selby* [1965, p. 334, no. 380]:

$$\phi_{iN}{}^k = -\frac{Q_i}{4\pi l_i}\left\{(\xi - y') \ln [x'^2 + (y' - \xi)^2] - 2\xi + 2|x'| \tan^{-1}\left(\frac{\xi - y'}{|x'|}\right)\right\}_0^{l_i} \tag{B2}$$

To obtain the correct form for $\phi_{iN}{}^k$ we must translate to x, y coordinates (see Figure B1) and then rotate to X, Y coordinates which results in an expression of the form

$$\phi_{iN}{}^k = Q_i f_{iN}{}^k(X, Y) \tag{B3}$$

Now consider the image arc as shown in Figure B2. Recall that the strength per unit line length along the image arc, m_s, is

$$m_s = \frac{Q_i}{l_i} \frac{d\xi}{ds} \tag{7}$$

and the integral for the head distribution, $\phi_{iI}{}^k$ at any point in the plane due to sources on S distributed according to m_s can be written

$$\phi_{iI}{}^k = K^k b^k h_{iI} = \frac{-Q_i}{2\pi l} \int_{S_1}^{S_2} \frac{d\xi}{ds} \ln r_p\ (\xi)\ ds \tag{8}$$

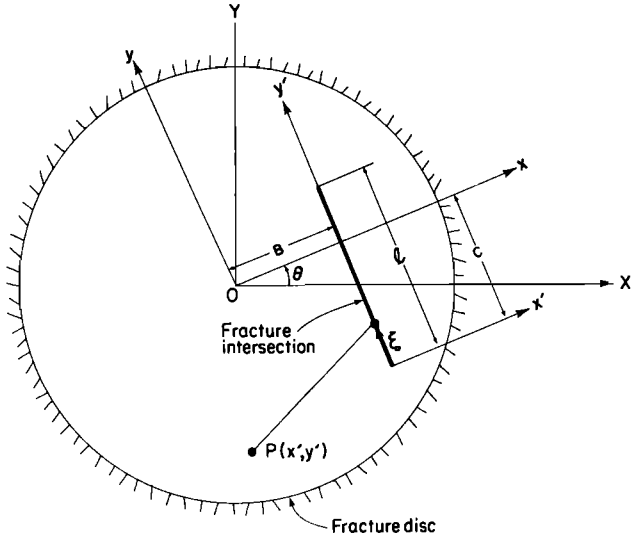

Fig. B1. Fracture intersection in a fracture disc.

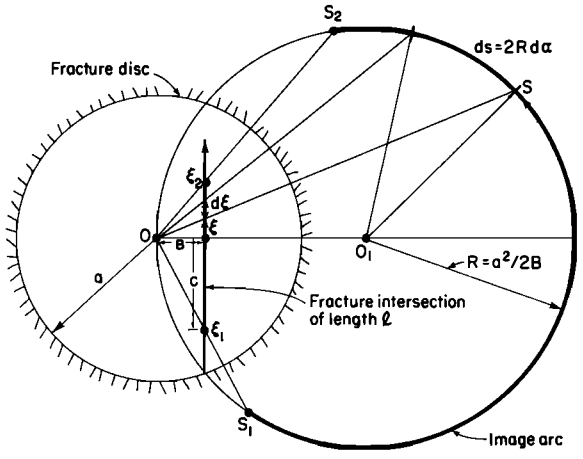

Fig. B2. Construction for calculating the distribution of strength along an image arc.

where r_p is the distance from a point S on the arc to any point P in the plane.

Figure B3 shows the coordinate systems used to evaluate this integral. We now write r_p as a function terms of ξ and integrate from ξ_1 to ξ_2. On S we have

$$x_s' = R\cos\theta' = \frac{a^2}{2B}\cos\theta'$$
$$y_s' = R\sin\theta' = \frac{a^2}{2B}\sin\theta' \tag{B4}$$

So ${r_p}^2$ is given by

$${r_p}^2 = (x' - R\cos\theta')^2 + (y' - R\sin\theta')^2 \tag{B5}$$

where (x', y') is any point in the plane. Now referring to Figure B3,

$$\begin{aligned}\cos\theta' &= \cos 2\alpha,\\ &= 1 - 2\sin^2\alpha,\\ &= 1 - 2\left(\frac{\xi^2}{\xi^2 + B^2}\right)\end{aligned} \tag{B6}$$

$$\begin{aligned}\sin\theta' &= \sin 2\alpha,\\ &= 2\sin\alpha\cos\alpha,\\ &= \frac{2\xi B}{\xi^2 + B^2}\end{aligned} \tag{B7}$$

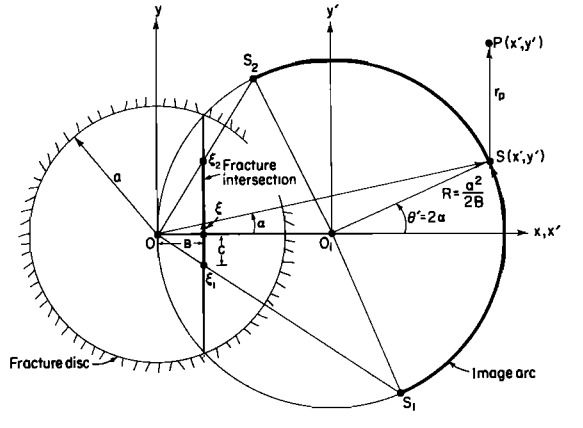

Fig. B3. Construction for calculation of potential due to sources on the image arc.

Substituting B6 and B7 into B5 gives

$${r_p}^2 = [(x'^2 + y'^2 + R^2 + 2Rx')\xi^2 - (4Ry'B)\xi + (x'^2 + y'^2 + R^2 - 2Rx')B^2][\xi^2 + B^2]^{-1} \tag{B8}$$

Now ${\phi_{iI}}^k$ can be written in terms of ξ. Substituting (B8) into (8) gives

$${\phi_{iI}}^k = K^k b^k h_{iI} = \frac{-Q_i}{4\pi l}\left\{\int_{\xi_1}^{\xi_2}\ln[\Omega]\,d\xi - \int_{\xi_1}^{\xi_2}\ln(\xi^2 + B^2)\,d\xi\right\} \tag{B9}$$

where

$$\begin{aligned}\Omega &= \gamma\xi^2 + \beta\xi + \alpha;\\ \gamma &= (x'^2 + y'^2 + R^2 + 2Rx');\\ \beta &= -(4Ry'B);\\ \alpha &= (x'^2 + y'^2 + R^2 - 2Rx')B^2.\end{aligned} \tag{B10}$$

These integrals can be evaluated using the work by *Selby* [1965, p. 334, no. 380]

$${\phi_{iI}}^k = K^k b^k \bar{h}_{iI} = \frac{-Q_i}{4\pi l_i}\left\{\left[\left(\xi + \frac{\beta}{2\gamma}\right)\ln\Omega + \frac{(4\alpha\gamma - \beta^2)^{1/2}}{\gamma}\tan^{-1}\left(\frac{2\gamma\xi + \beta}{(4\alpha\gamma - \beta^2)^{1/2}}\right)\right] - \left[\xi\ln(\xi^2 + B^2) + 2B\tan^{-1}\left(\frac{\xi}{B}\right)\right]\right\}_{\xi_1}^{\xi_2} \tag{B11}$$

Finally, (B11) must be translated to x, y coordinates and then rotated to X, Y coordinates. After this substitution we have

$${\phi_{iI}}^k = K^k b^k {\bar{h}_{iI}}^k = Q_i {f_{iI}}^k(X, Y) \tag{B12}$$

APPENDIX C

Radial Intersections

If the intersection is radial, a different form must be used for ${\phi_{iN}}^k$ and ${\phi_{iI}}^k$. Figure C1 shows the geometry for this case. For ${\phi_{iN}}^k$, the potential due to the sources on the radial node, we have

$${\phi_{iN}}^k = K^k b^k \bar{h}_{iN} = \frac{-Q_i}{2\pi l_i}\int_{\xi_1}^{\xi_2}\frac{1}{2}\ln[(x - \xi)^2 + y^2]\,d\xi \tag{C1}$$

This integral is evaluated by the same formula as for a nonradial node:

$${\phi_{iN}}^k = \frac{-Q_i}{4\pi l}\left\{(\xi - x)\ln[(x - \xi)^2 + y^2] - 2\xi + 2|y|\tan^{-1}\left(\frac{\xi - x}{|y|}\right)\right\}_{\xi_1}^{\xi_2} \tag{C2}$$

which again must be written in X, Y coordinates.

The image of a radial node is also a radial line segment extending from $x = a^2/\xi_1$ to $x = a^2/\xi_2$. First, we evaluate the strength per unit length, m_η. Referring to Figure (C1),

$$m_\eta = m_\xi\frac{d\xi}{d\eta} = \frac{Q_i}{l_i}\frac{d\xi}{d\eta} \tag{C3}$$

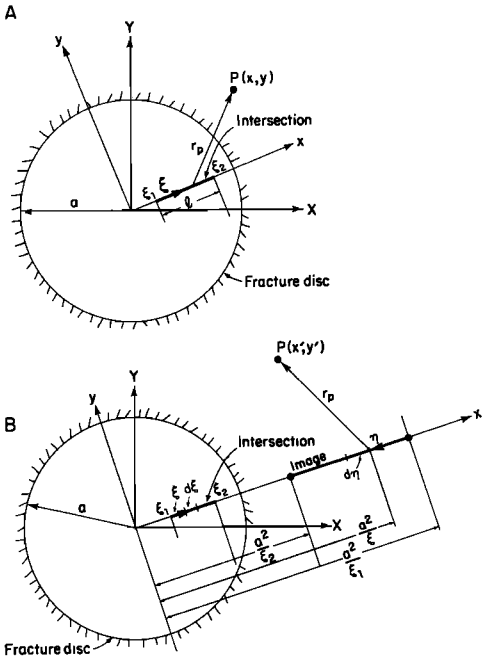

Fig. C1. (*a*) Radial intersection and (*b*) radial image.

The distance from a point on the image to any point $P(x', y')$ is

$$r_p^2 = \left[\left(x - \frac{a^2}{\xi}\right)^2 + y^2\right] = \frac{(x^2 + y^2)\xi^2 - 2a^2x\xi + a^4}{\xi^2} \tag{C4}$$

So

$$\phi_{iI}{}^k = -\frac{Q_i}{4\pi l_i}\int_0^{(a^2/\xi_1 - a^2/\xi_2)} \frac{d\xi}{l\eta} \ln r_p \, d\eta$$

$$= \frac{-Q_i}{4\pi l_i}\left(\int_{\xi_1}^{\xi_2} \ln \Omega \, d\xi - \int_{\xi_1}^{\xi_2} 2 \ln \xi \, d\xi\right) \tag{C5}$$

where

$$\begin{aligned} \Omega &= \alpha + \beta\xi + \gamma\xi^2 \\ \alpha &= a^4 \\ \beta &= -2a^2x \\ \gamma &= (x^2 + y^2) \end{aligned} \tag{C6}$$

The integration yields

$$\phi_{iI}{}^k = K^k b^k \bar{h}_{iI} = \frac{-Q_i}{4\pi l_i}\left\{\left[\left(\xi + \frac{\beta}{2\gamma}\right)\ln \Omega - 2\xi + \frac{(4\gamma\alpha - \beta^2)^{1/2}}{\gamma}\tan^{-1}\left(\frac{2\gamma\xi + b}{(4\gamma\alpha - \beta^2)^{1/2}}\right)\right] - 2[\xi \ln \xi - \xi]\right\}_{\xi_1}^{\xi_2} \tag{C7}$$

Finally, the rotation of coordinates is applied and the potential contribution of node i is of the form

$$\phi_i{}^k = Q_i f_{iN}{}^k(X, Y) + \Theta f_{iL}{}^k(X, Y) + Q_i f_{iI}{}^k(X, Y) \tag{C8}$$

NOTATION

a radius of a fracture, $[L]$.
b^k effective hydraulic aperture of fracture k, $[L]$.
C^k datum head in fracture k $[L]$.
$f_{iN}{}^k(X, Y)$ geometric function, $\phi_{iN}{}^k = Q_i f_{iN}{}^k$, $[L]$.
$f_{iI}{}^k(X, Y)$ geometric function, $\phi_{iI}{}^k = Q_i f_{iI}{}^k$, $[L]$.
$F_i{}^k(X, Y)$ geometric function, $F_i{}^k = f_{iN}{}^k + f_{iI}{}^k$, $[L]$.
$\mathscr{F}_{ij}{}^k$ matrix of shape functions for average head on node j due to the presence of node i.
$\mathscr{G}_{ij}{}^k = [\zeta_{ij}{}^k]^{-1}$.
h hydraulic head, $[L]$.
$\bar{h}_i$ average head on node i, $[L]$.
H_i prescribed head on boundary node i, $[L]$.
I subscript to reference the contribution of an image.
K permeability of a fracture $K = b\rho g/12\mu$, $[L/T]$.
k superscript for fracture k.
m strength of a source, $[L^3/T]$.
m_ξ strength per unit length on the node, $[L^2/T]$.
m_s, m_η strength per unit length on an image (nonradial and radial respectively), $[LT]$.
n total number of intersections on fracture k.
N subscript to reference the contribution of a node.
i, j subscripts to reference node numbers.
r_p distance from a point on a line source to any point in the plane, $[L]$.
S an arc which is the locus of images for a nonradial intersection.
s variable of integration on the image of a nonradial node, $[L]$.
Q flux, $[L^3/T]$.
Q_T total flux through the face of a cubic region of fractured rock, $[L^3/T]$.
w width of a node, $[L]$.
ε small distance, $[L]$.
$\zeta_{ij}{}^k$ matrix of shape factors, $\zeta_{ij}{}^k = [(\mathscr{F}_{ij}{}^k - \mathscr{F}_{nj}{}^k) - (\mathscr{F}_{ij+1}{}^k - \mathscr{F}_{nj+1}{}^k)]$.
η variable of integration on the image of a radial node, $[L]$.
ξ variable of integration along a line source, $[L]$.
ϕ potential, $\phi = Kbh$, $[L^3/T]$.
$\phi_{iN}{}^k(X, Y)$ potential contribution of sources on intersection i in fracture k, $[L^3/T]$.
$\phi_{iI}{}^k(X, Y)$ potential contribution of sources of the image of intersection i in fracture k, $[L^3/T]$.
$\phi_i{}^k(X, Y)$ potential due to node i and its image in fracture k, $[L^3/T]$.
$\Phi^k(X, Y)$ total potential in fracture k, $[L^3/T]$.
$\bar{\Phi}_i{}^k$ average of total potential on node i in fracture k, $[L^3/T]$.

Acknowledgments. We would like to thank F. Sisto for his help in identifying the use of image theory to solve this problem. We are also indebted to I. Javendel for his help and comments. Many thanks to E. Klahn for typing and retyping this manuscript. This work was supported by the U. S. Department of Energy, Chicago Operations Office for the Crystalline Rock Project (CPO), Task E504-621AH under Contract DE-AC03-76SF00098.

REFERENCES

Baecher, G. B., and N. A. Lanney, Trace length biases in joint surveys, in *Proceedings of the 19th U.S. Symposium on Rock Mechanics*, pp. 56–65, American Institute of Mining Engineers, New York, 1978.

Barton, C. C., Tectonic significance of fractures in welded tuff, Yucca Mountain, Southwest Nevada, *Abstr. Prog.*, *16*(6), 1984.

Conrad, F., and C. Jacquin, Representation of a two-dimensional fracture network by a probabilistic model: Application to calculation of the geometric magnitude of matrix blocks, *Publ. UCRL-*

Trans-10814, 75 pp., Univ. of Calif., Lawrence Livermore Lab., Berkeley, 1973.

Dershowitz, W. S., Rock Joint Systems, Ph.D. thesis, Dept. of Civ. Eng., Mass. Inst. of Technol., Cambridge, 1984.

Hudson, J. A., and S. D. Priest, Discontinuities and rock mass geometry, *Int. J. Rock Mech. Min. Sci. Geomech. Abstr.*, *16*, 135–148, 1979.

LaPointe, P. R., and J. A. Hudson, Characterization and Interpretation of Rock Mass Jointing Patterns, Dep. of Metall. and Miner. Eng., Univ. of Wisc., Madison, 1981.

Long, J. C. S., Investigation of Equivalent Porous Medium Permeability in Networks of Discontinuous Fractures, Ph.D. thesis, Coll. of Eng., Univ. of Calif., Berkeley, 1983.

Long, J. C. S., and P. A. Witherspoon, The relationship of the degree of interconnection and permeability in a fracture network, *J. Geophys. Res.*, *90*, 3087–3098, 1985.

Long, J. C. S., J. S. Remer, C. R. Wilson, and P. A. Witherspoon, Porous media equivalents for networks of discontinuous fractures, *Water Resour. Res.*, *18*(3), 645–658, 1982.

Long, J. C. S., H. K. Endo, K. Karasaki, L. Pyrak, P. Maclean, and P. A. Witherspoon, Hydrologic behavior of fracture networks, paper presented at Proceedings of the International Association of Hydrogeologists 17th International Congress, Intl. Assoc. Hydrogeol., Tucson, Ariz., January 7–10, 1985.

Mahtab, M. A., and F. M. Yegulalp, A rejection criterion for definition of clusters in orientation data, in *Proceedings, 23rd Symposium on Rock Mechanics*, University of California, Berkeley, 1982.

Mahtab, M. A., D. B. Bolstad, J. R. Alldredge, and R. J. Shanley, Analysis of fractured orientations for input to structural models of discontinuous rock, *Invest. Rep. 7669*, 76 pp., Bur. of Mines, U.S. Dep. of the Int., 1972.

Milne-Thomson, R. M., *Theoretical Hydrodynamics*, MacMillan, New York, 1968.

Pincus, H. J., The analysis of aggregates of orientation data in the earth sciences, *J. Geol.*, *61*(6), 482–509, 1953.

Pollard, D. D., On the form and stability of open hydraulic fractures in the earth's crust, *Geophys. Res. Lett.*, *3*(9), 513–516, 1976.

Robertson, A., The interpretation of geological factors for use in slope stability, paper presented at the Symposium on the Theoretical Background to the Planning of Open Pit Mines With Special Reference to Slope Stability, South African Inst. of Min. and Metall., Johannesburg, 1970.

Selby, S. M. (Ed.), *Standard Mathematical Tables*, 14th ed., The Chemical Rubber Co., Cleveland, Ohio, 1965.

Snow, D. T., Anisotropic permeability of fractured media, *Water Resour. Res.*, *5*(6), 1273–1289, 1969.

Veneziano, D., Probabilistic model of joints in rock, technical report, 4 pp., Civ. Eng. Dep. Mass. Inst. of Technol., Cambridge, 1979.

P. Gilmour, J. C. S. Long, and P. A. Witherspoon, Earth Sciences Division, Lawrence Berkeley Laboratory, University of California, Berkeley, CA 94720.

(Received November 1, 1983;
revised March 25, 1985;
accepted April 9, 1985.)